Supplementary Material for

Endo-exo classification of episodic rock creep in underground mines: Implications for forecasting catastrophic failure

Qinghua Lei[1], Daniel Francois Malan[2], Didier Sornette[3]

[1]*Department of Earth Sciences, Uppsala University, Sweden*
[2]*Department of Mining Engineering, University of Pretoria, Hatfield, South Africa*
[3]*Institute of Risk Analysis, Prediction and Management, Academy for Advanced Interdisciplinary Studies, Southern University of Science and Technology, Shenzhen, China*

Contents of this file

Introduction

This document provides supplementary information to complement the results and discussions in the main paper. Fig. S1 shows the layout of UG2 panels mined toward and below a Merensky remnant. Fig. S2 illustrates the field setup and operational mechanisms of the clockwork closure meters. Fig. S3 shows the location of Panel 1N with respect to the Merensky remnant. Fig. S4 shows the typical ground conditions in Panel 1N. Fig. S5 shows the location of Panel 4S with respect to the Merensky remnant. Fig. S6 presents a photo of Panel 5S which collapsed on 17 October 2005. Fig. S7 presents a photo of Panel 7N which collapsed on 04 April 2007. Fig. S8-S10 present sensitivity analyses of the random walk simulations with varying initial stress levels.

Fig. S1. UG2 panels mined toward and below a Merensky remnant.

(a) (b)

(c)

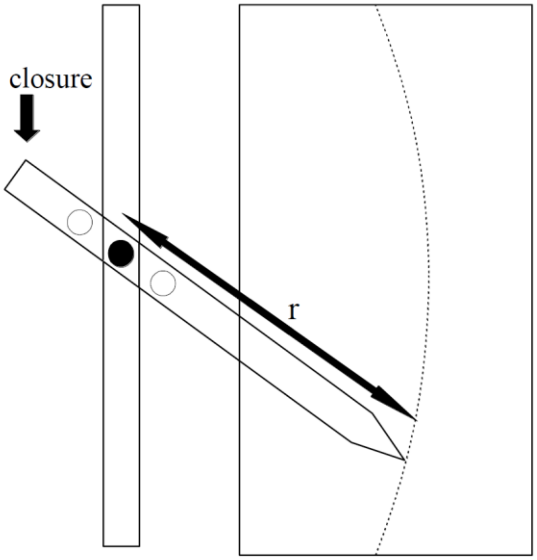

Fig. S2. Photographs of a clockwork closure meter (a) in a closed box and (b) with the box open to reveal the mechanism, which is further illustrated in (c). It is composed of two pipes, one of which slides within the other under the resistance of a spring. The base of the instrument is attached to the lower pipe, while a guide affixed to the upper pipe moves the needle. The instrument is set up with the needle tip positioned near the lower edge of the drum's graph paper. The stope closure forces the upper pipe deeper into the lower pipe, causing the needle to move upwards on the paper. The needle arm features multiple pivot points, enabling adjustable amplification of the measured closure magnitude. The clock completes one full rotation over a certain period, producing a continuous record of the closure throughout that time. The raw data need to be corrected before use and more details of the correction method can be found in Malan (1998).

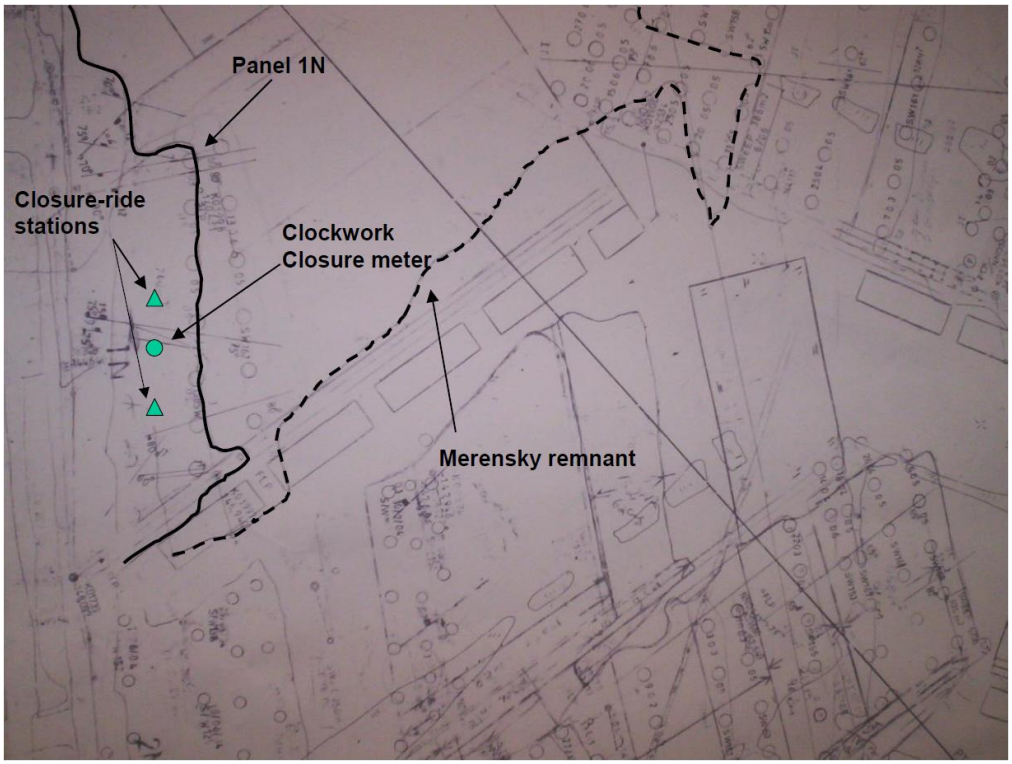

Fig. S3. Location of Panel 1N with respect to the Merensky remnant.

Fig. S4. Typical ground conditions in Panel 1N.

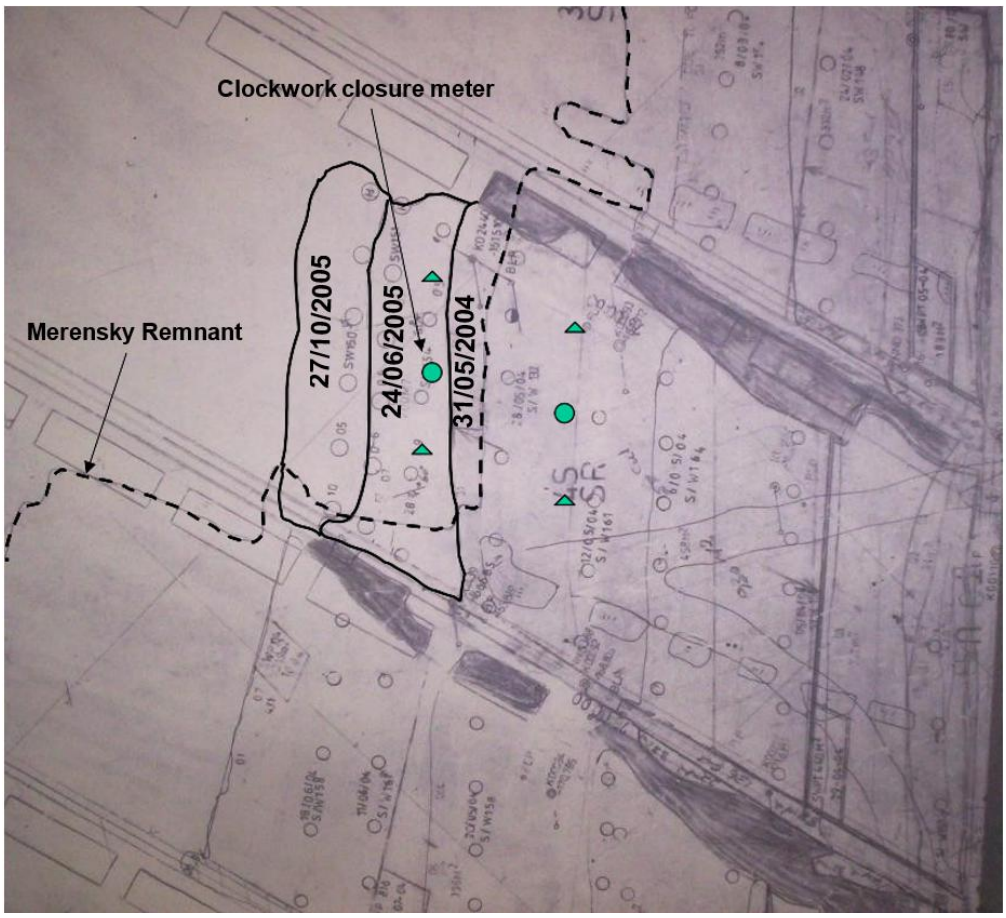

Fig. S5. Location of Panel 4S with respect to the Merensky remnant.

Fig. S6. Collapse in Panel 5S on 17 October 2005.

Fig. S7. Collapse in Panel 7N on 04 April 2007.

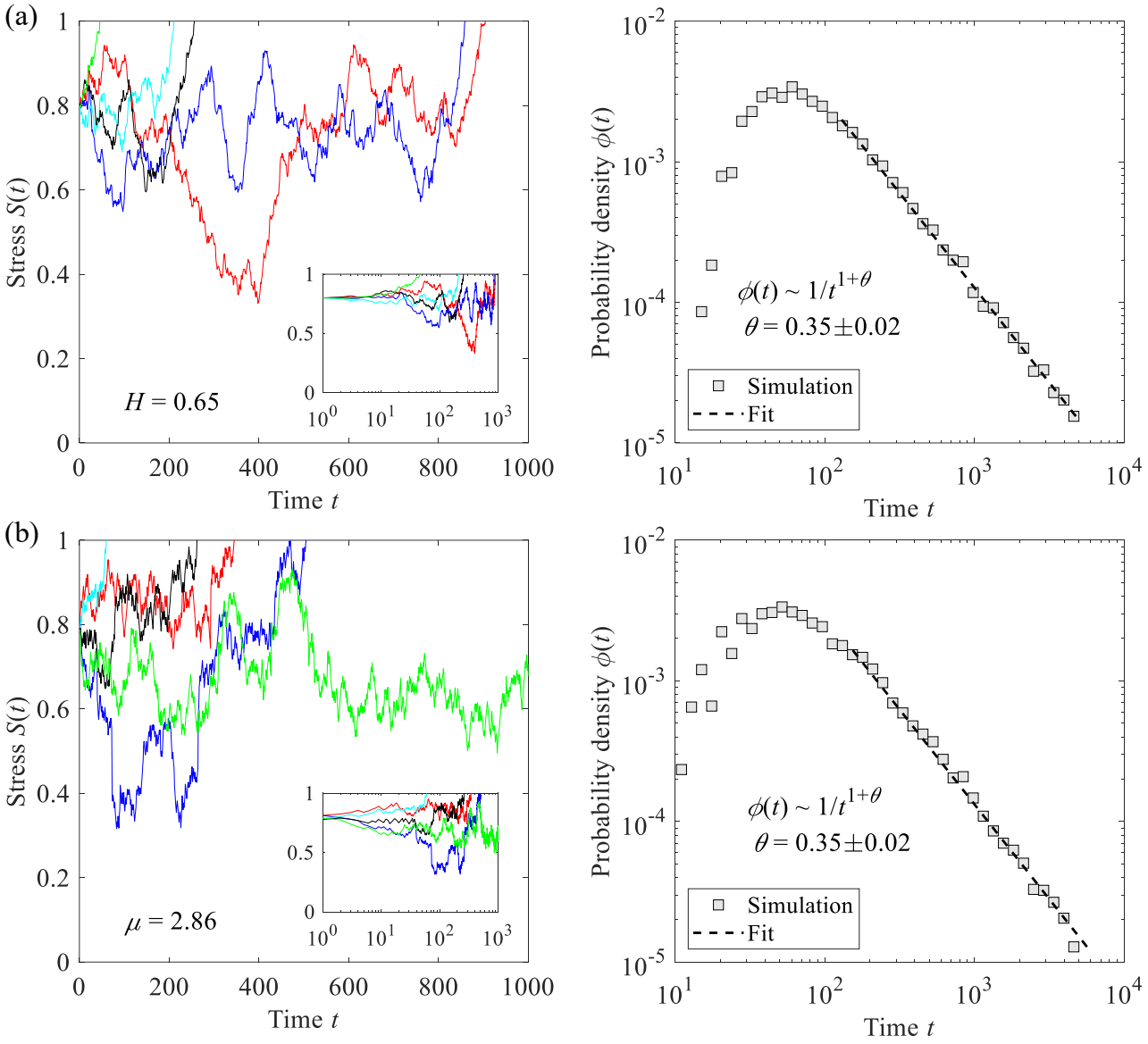

Fig. S8. Random walk simulations of stress fluctuations with increments s (a) obeying a fractional Brownian motion with a Hurst exponent of $H = 0.65$ and a characteristic increment amplitude of $s^* = 0.01$, or (b) drawn from a Pareto distribution with a shape parameter of $\mu = 2.86$ and a minimum increment size of $s_{\min} = 0.01$. In the simulation, stress $S(t)$ evolves as a random walk starting from an initial value $S_0 = 0.8$ with each step taking a unit time, and the process stops until $S(t)$ for the first time exceeds the critical threshold $S_c = 1.0$. Left panels give the stress trajectories of 5 realizations which are arbitrarily selected from 10000 simulated realizations; the inset displays the same data with a logarithmic time scale. Right panels show the probability density function of waiting times $\phi(t) \propto 1/t^{1+\theta}$, derived from the random walk simulations, with $\theta = 0.35$ obtained for both models.

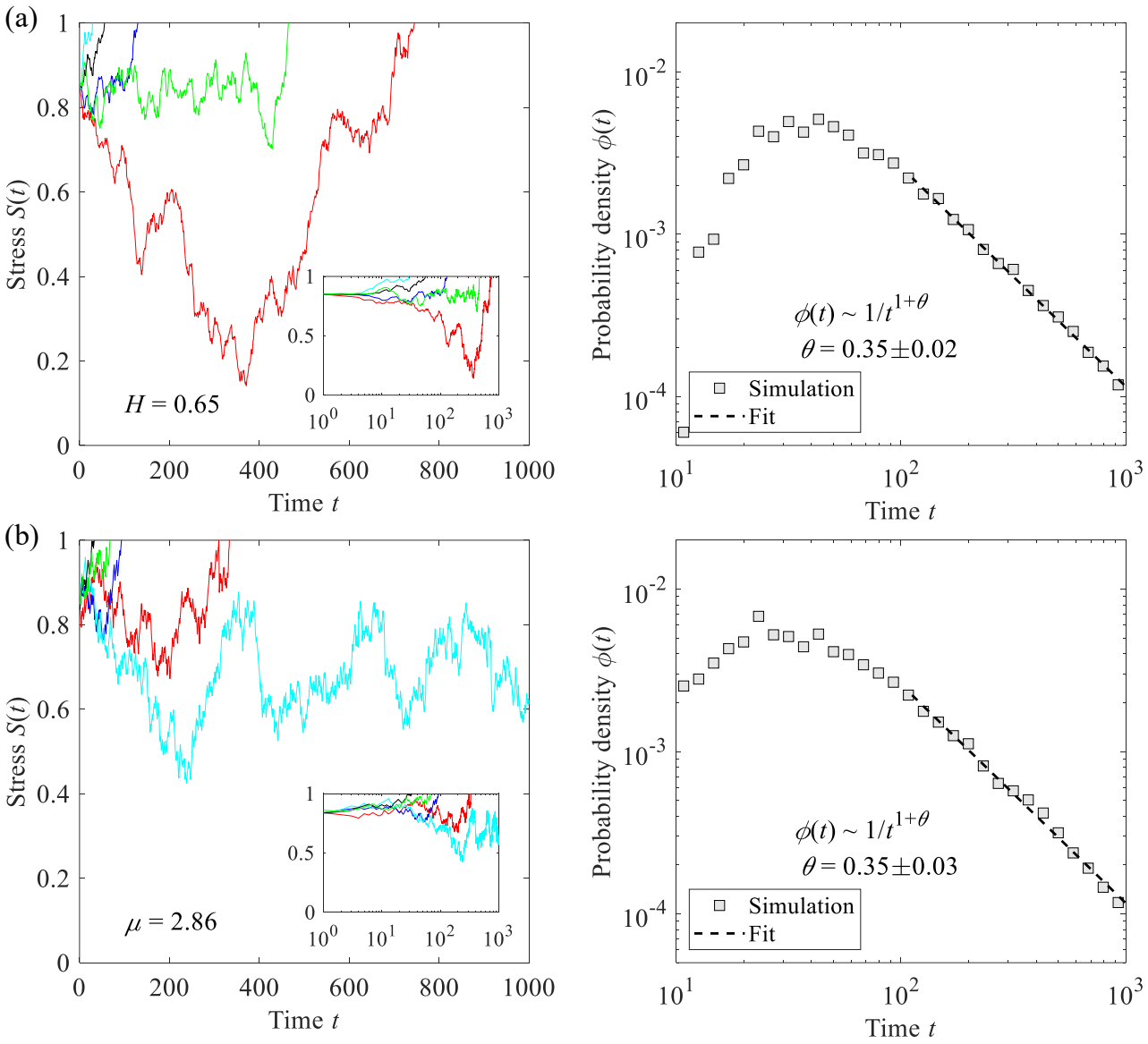

Fig. S9. Random walk simulations of stress fluctuations with increments s (a) obeying a fractional Brownian motion with a Hurst exponent of $H = 0.65$ and a characteristic increment amplitude of $s^* = 0.01$, or (b) drawn from a Pareto distribution with a shape parameter of $\mu = 2.86$ and a minimum increment size of $s_{\min} = 0.01$. In the simulation, stress $S(t)$ evolves as a random walk starting from an initial value $S_0 = 0.85$ with each step taking a unit time, and the process stops until $S(t)$ for the first time exceeds the critical threshold $S_c = 1.0$. Left panels give the stress trajectories of 5 realizations which are arbitrarily selected from 10000 simulated realizations; the inset displays the same data with a logarithmic time scale. Right panels show the probability density function of waiting times $\phi(t) \propto 1/t^{1+\theta}$, derived from the random walk simulations, with $\theta = 0.35$ obtained for both models.

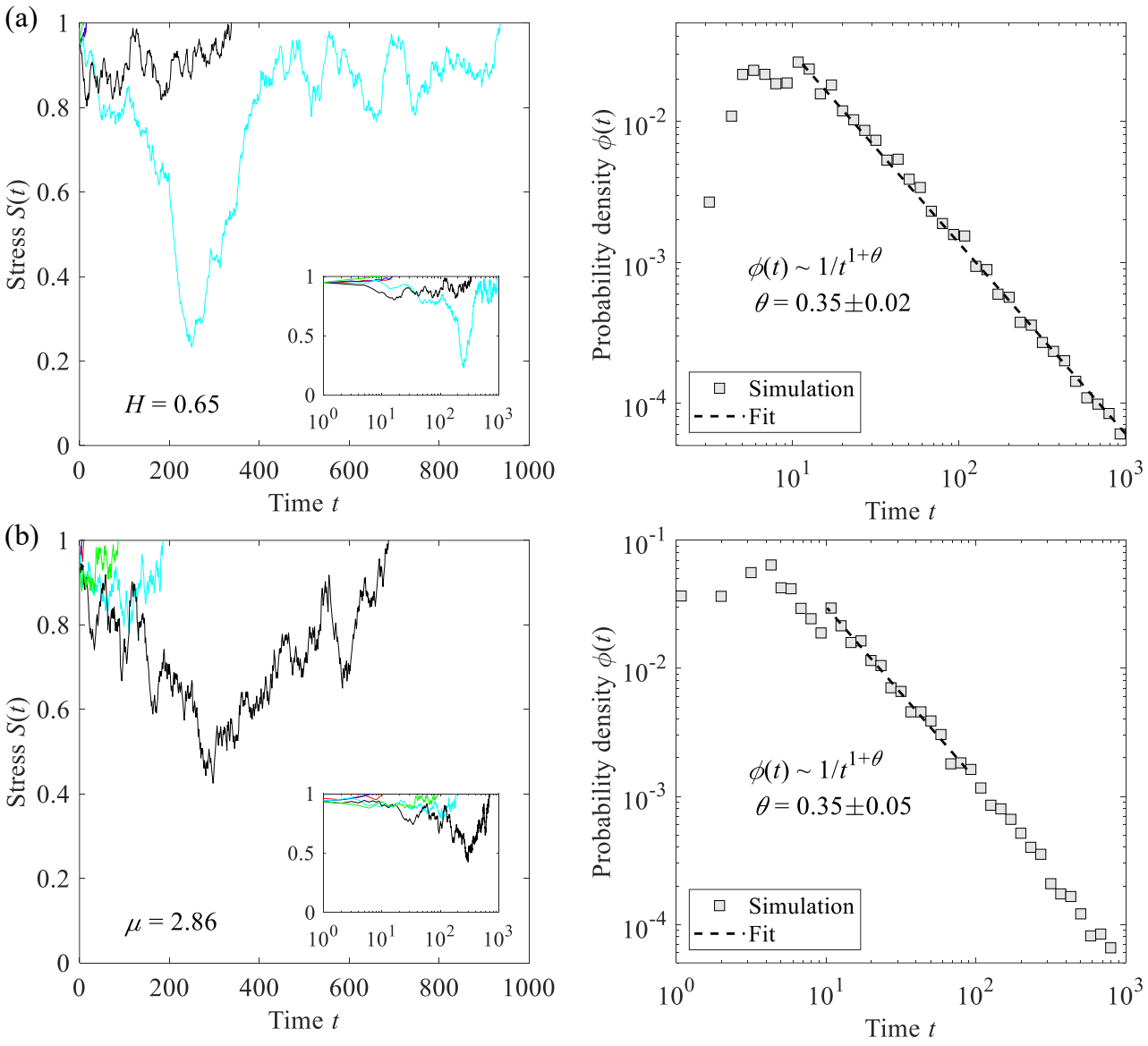

Fig. S10. Random walk simulations of stress fluctuations with increments s (a) obeying a fractional Brownian motion with a Hurst exponent of $H = 0.65$ and a characteristic increment amplitude of $s^* = 0.01$, or (b) drawn from a Pareto distribution with a shape parameter of $\mu = 2.86$ and a minimum increment size of $s_{\min} = 0.01$. In the simulation, stress $S(t)$ evolves as a random walk starting from an initial value $S_0 = 0.95$ with each step taking a unit time, and the process stops until $S(t)$ for the first time exceeds the critical threshold $S_c = 1.0$. Left panels give the stress trajectories of 5 realizations which are arbitrarily selected from 10000 simulated realizations; the inset displays the same data with a logarithmic time scale. Right panels show the probability density function of waiting times $\phi(t) \propto 1/t^{1+\theta}$, derived from the random walk simulations, with $\theta \approx 0.35$ obtained for both models. Note that the upper bound for the power law fit in (b) is estimated as $t_{\text{cross}} \approx [(S_c - S_0)/s_{\min}]^{\mu} = 100$.